*J. Fluid Mech.* (2010), *vol.* 643, *pp.* 479–494.  
doi:10.1017/S0022112009992308

# How long are tidal channels?

G. SEMINARA[1], S. LANZONI[2], N. TAMBRONI[1]† AND M. TOFFOLON[3]

[1]Department of Civil and Environmental Engineering, University of Genova, via Montallegro 1, 16145 Genova, Italy

[2]Dipartimento di Ingegneria Idraulica, Marittima, Ambientale e Geotecnica, University of Padova, via Loredan 20, 35131 Padova, Italy

[3]Department of Civil and Environmental Engineering, University of Trento, via Mesiano 77, 38100 Trento, Italy

(Received 18 December 2008; revised 18 September 2009; accepted 21 September 2009; first published online 23 November 2009)

Do tidal channels have a characteristic length? Given the sediment characteristics, the inlet conditions and the degree of channel convergence, can we predict it? And how is this length affected by the presence of tidal flats adjacent to the channel? We answer the above questions on the basis of a fully analytical treatment, appropriate for the short channels typically observed in coastal wetlands. The equilibrium length of non-convergent tidal channels is found to be proportional to the critical flow speed for channel erosion. Channel convergence causes concavity of the bed profile. Tidal flats shorten equilibrium channels significantly. Laboratory and field observations substantiate our findings.

**Key words:** channels, morphodynamic equilibrium, tides

## 1. Introduction

We are concerned with tidal channels which typically form networks issuing from tidal inlets of back-barrier lagoons (figure 1*a*). In these settings, proceeding in the landward direction, channel width, channel depth and grain size decrease, while the tide is allowed to expand into shallow regions (tidal flats) adjacent to the channel, which eventually merge into vegetated salt marshes, submerged during part of the tidal cycle only.

The issue of long-term equilibrium of tidal patterns is a delicate one. Let us focus on the simplest case of a tidal channel connected to the sea through a tidal inlet and let us define 'morphodynamic equilibrium' as a state characterized by the condition that the bed elevation undergoes no net variation in a tidal cycle. Then, the first necessary condition for equilibrium is that no net import of sediments from (or export to) the sea must occur in a tidal cycle. Provided this condition is satisfied, tidal channels achieve equilibrium adjusting their bed profiles and lengths to the asymptotic condition that the net sediment flux in a tidal cycle must eventually vanish everywhere: this will be called a condition of static equilibrium. And, indeed, the laboratory experiments of Tambroni, Bolla & Seminara (2005) and the numerical simulations of Lanzoni & Seminara (2002) and Todeschini, Toffolon & Tubino (2008) do suggest that static equilibrium is eventually reached under the conditions stated above. Moreover, field

† Email address for correspondence: nicoletta.tambroni@unige.it

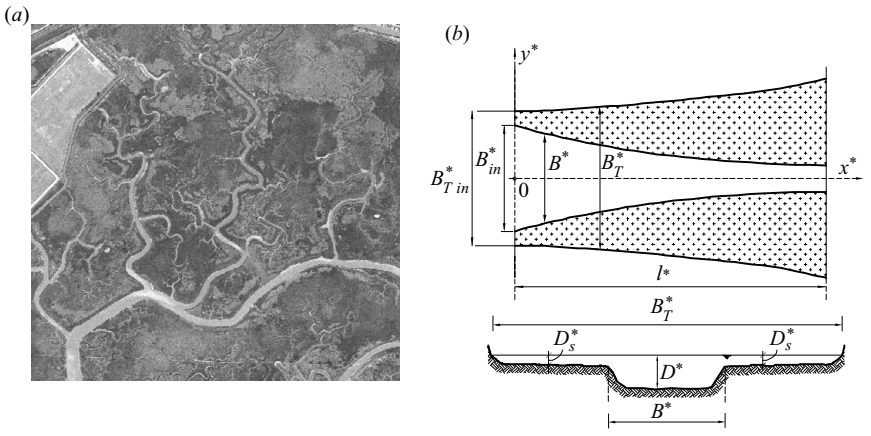


FIGURE 1. (*a*) Tidal channels with adjacent tidal flats in Venice lagoon; (*b*) sketch of a tidal convergent channel with adjacent shoals.

data (D'Alpaos *et al.* 2009) support the idea that channel networks of back-barrier lagoons do approach equilibrium. Viewed on a larger time scale the problem is even more delicate as sea level rise and subsidence also play a role. In these tidal environments, suggestions have been made that accretion often balances relative sea level rise (Nichols & Boon 1994) and an essentially stable configuration is attained by dead end tidal creeks dissecting salt marshes as well as by channels departing from the barrier inlets and innervating the adjacent tidal flats.

A different notion of equilibrium, that we will call dynamic equilibrium, has been investigated by Pritchard & Hogg (2003) who considered intertidal mud flats located along sheltered portions of coasts and estuaries. In these tidal settings the flats typically prograde (or retreat) as a consequence of a net import of sediments from (or export to) the offshore region. This migration process occurs very slowly (on a time scale of the order of thousands of tidal cycles) implying that the residual fluxes associated with advance (retreat) are much smaller than the instantaneous flux. A dynamic equilibrium profile is then attained with a sediment flux approximately constant throughout the flat, i.e. with a peak shear stress uniformly distributed along the flat (Friedrichs & Aubrey 1996; Pritchard & Hogg 2003).

In the present paper we focus on static equilibrium of tidal channels. A number of ingredients affect this equilibrium state. The nature of sediments (cohesionless versus cohesive) controls bed erodibility. Channel convergence, the characteristics of the forcing oscillation and the presence of tidal flats, exchanging water and sediments with the channel, control the hydrodynamics. Inlet geometry affects the ability of the water body feeding the channel to exchange sediments through the inlet. Finally, channel curvature is known to affect the lateral bottom equilibrium (Solari *et al.* 2002), while tidal bedforms (Seminara & Tubino 2001) likely play a minor role, which is disregarded below. The subject has been recently reviewed by de Swart & Zimmermann (2009). The general picture of the process whereby equilibrium is established, arising from theory, computations and laboratory observations, is as follows: starting from an initially horizontal bed profile, a sediment wave propagates landwards in the channel leading to bed emergence and shore development inwards.

A natural yet fundamental question then arises: can we predict the length of tidal channels? In other words, given the sediment characteristics, the inlet conditions and the degree of channel convergence, can we predict the channel length? And what is the role of tidal flats?

We show below that answers to the above questions can indeed be given on the basis of a fully analytical treatment, appropriate for channels and flats sufficiently short relative to the length of the tidal wave (§ 2), a condition first employed by Schuttelaars & de Swart (1996), which justifies a perturbative solution of the governing equations (§ 3). The novel feature of the present approach is that our inner boundary condition allows for the existence of a dry and wet region, which is treated as an inner layer in the language of matched asymptotics. We are then able to determine a fully analytical solution valid throughout the channel and impose the condition of morphodynamic equilibrium to determine the shape and length of the equilibrium profile (§ 4). Finally, we investigate the role of tidal flats (§ 5), modelled as rectangular and aligned with the channel, accounting for their storage effect and ignoring their dynamic effect: tidal flats are thus found to enhance the flow speed in the channel, reduce its equilibrium length and enhance its concavity.

Note that the short channel assumption is quite well satisfied throughout the networks of most coastal wetlands. On the contrary, long estuaries are excluded from the present analysis though, as discussed in § 6, the ideas developed herein may be found of some relevance also for estuarine environments.

## 2. Mathematical formulation of the problem

We consider a straight tidal channel of length $l^*$ (hereafter a star superscript will denote dimensional quantities), rectangular cross-section and width $B^*$ varying exponentially landwards as typical of tidal environments (Friedrichs & Aubrey 1994):

$$B^* = B^*_{in} \exp(-x^*/l^*_b). \tag{2.1}$$

Here $l^*_b$ is the convergence length, $B^*_{in}$ the inlet width and $x^*$ a longitudinal coordinate pointing landwards with origin at the inlet (figure 1*b*). In the context of a one-dimensional model the motion of the fluid phase is governed by the classical continuity and de Saint Venant equations, which express the principles of mass and momentum conservation. It is convenient herein to set the latter equations in dimensionless form. Below, $t^*$ denotes time, $D^*$ and $U^*$ are the cross-sectionally averaged flow depth and flow speed respectively, $H^*$ is the water surface elevation relative to the mean sea level and $g$ is gravity. The relevant variables are scaled as follows:

$$x^* = l^* x, \quad t^* = \omega_0^{*-1} t, \tag{2.2}$$

$$H^* = a_0^* H, \quad D^* = \mathscr{D}_0^* D, \quad U^* = \mathscr{U}_0^* U. \tag{2.3}$$

In (2.2), (2.3) $\omega_0^*$ and $a_0^*$ are angular frequency and amplitude of the forcing tide, $\mathscr{D}_0^*$ is a typical depth, taken equal to the inlet depth scale and $\mathscr{U}_0^* (= \epsilon \sqrt{g \mathscr{D}_0^*})$ is a characteristic speed, with $\epsilon$ relative tidal amplitude ($\epsilon = a_0^*/\mathscr{D}_0^*$). The above scaling is appropriate everywhere along the channel, except in the landward region where the bed emerges during part of the tidal cycle, hence the flow depth approaches zero. Here, the flow depth scales with the tidal amplitude $a_0^*$: indeed, this inner region behaves as a boundary layer where rescaling will be necessary.

At this stage, we ignore tidal flats, an assumption that will be relaxed in § 5. Moreover, we neglect dissipative effects. In § 6 we will discuss how severe is this assumption in practice. With the above notations the governing equations read:

$$\lambda \frac{\partial D}{\partial t} + \epsilon \frac{\partial (UD)}{\partial x} - \epsilon \lambda_b (UD) = 0, \tag{2.4}$$

$$\lambda \frac{\partial U}{\partial t} + \epsilon U \frac{\partial U}{\partial x} + \frac{\partial H}{\partial x} = 0 \tag{2.5}$$

with $\lambda$ the ratio between channel length and inviscid wavelength of a small-amplitude tidal wave and $\lambda_b$ weighing the relative effect of channel convergence:

$$\lambda = \frac{l^* \omega_0^*}{\sqrt{g \mathscr{D}_0^*}}, \quad \lambda_b = \frac{l^*}{l_b^*}. \tag{2.6}$$

Equations (2.4) and (2.5) must be supplemented by appropriate boundary conditions. At the channel mouth we set

$$D|_{x=0} = 1 + \epsilon H(x,t)|_{x=0} = 1 + \epsilon f(t). \tag{2.7}$$

The landward boundary condition requires more care: in fact, the shoreline, located at $x_{sh}^*(t^*)$, is a moving boundary through which no relative flux may occur, hence:

$$U|_{x=x_{sh}} = \frac{\lambda}{\epsilon} \dot{x}_{sh}, \quad D|_{x=x_{sh}} = 0. \tag{2.8}$$

In a channel with erodible bed, flow depth and free surface elevation are independent variables. Hence, in order to close the mathematical formulation we need to couple hydrodynamics to morphodynamics through the one-dimensional form of the evolution equation of the bed interface, expressing mass conservation of the solid phase (Exner 1925), which reads

$$B^* \frac{\partial (\bar{c} D^*)}{\partial t^*} + (1-p) B^* \frac{\partial \eta^*}{\partial t^*} + \frac{\partial (B^* q_s^*)}{\partial x^*} = 0, \tag{2.9}$$

where $\eta^*$ is the local and instantaneous value of the laterally averaged bed elevation, $\bar{c}$ is the sediment concentration averaged over the cross-section, $p$ is sediment porosity, $q_s^*$ is the total sediment flux per unit width (transported as both bedload and suspended load). At static equilibrium, each property of both the flow field and the sediment motion cannot exhibit net variations in a tidal cycle. This applies in particular to bed elevation (hence to the position of the shoreline), sediment concentration and flow depth. Integrating (2.9) in a tidal period, one finds

$$\int_{t^*}^{t^*+T^*} \frac{\partial (B^* q_s^*)}{\partial x^*} \, \mathrm{d}t^* = \frac{\partial \left( B^* \int_{t^*}^{t^*+T^*} q_s^* \, \mathrm{d}t^* \right)}{\partial x^*} = 0. \tag{2.10}$$

Hence, the net sediment flux in a tidal cycle must be constant throughout the channel and the constant must vanish in order to satisfy the landward boundary condition.

## 3. An analytical solution for short channels

We now set

$$\lambda = \Lambda \epsilon, \quad \lambda_b \sim O(1) \tag{3.1}$$

with $\Lambda$ an $O(1)$ quantity. These assumptions are appropriate for typical channels of Venice lagoon with lengths $<10$ km, inlet depth $D_{in}^* < 10$ m and tidal amplitude $a_0 = 0.4$ m.

With the help of (3.1), the governing equations (2.4), (2.5) take the form

$$\Lambda \frac{\partial D}{\partial t} + \frac{\partial (UD)}{\partial x} - \lambda_b (UD) = 0, \tag{3.2}$$

$$\Lambda \frac{\partial U}{\partial t} + U \frac{\partial U}{\partial x} + \frac{1}{\epsilon} \frac{\partial H}{\partial x} = 0. \tag{3.3}$$

We now distinguish between an *outer region* where $(x-1) \sim O(1)$ and an *inner region* where $(x-1) \sim O(\epsilon)$, solve the problem distinctly in the two regions and then match the inner and outer solutions following the method of matched asymptotic expansions (Nayfeh 1973).

### 3.1. *The solution in the outer region:* $(x-1) \sim O(1)$, $D \sim O(1)$

An order of magnitude analysis of the fundamental equations suggests the following expansions:

$$D = D_0(x) + \epsilon D_1(x) + \epsilon H(x,t) + O(\epsilon^2), \tag{3.4}$$

$$(H, U/\epsilon) = [H_1(x,t), U_1(x,t)] + \epsilon [H_2(x,t), U_2(x,t)] + O(\epsilon^2). \tag{3.5}$$

Substituting from the latter expansions into the governing equations (3.2), (3.3) at leading order we find:

$$\frac{\partial H_1}{\partial x} = 0, \quad \frac{\partial (D_0 U_1)}{\partial x} - \lambda_b (D_0 U_1) = -\Lambda \frac{\partial H_1}{\partial t} \tag{3.6}$$

to be solved with the boundary condition

$$H_1|_{x=0} = f(t) \tag{3.7}$$

along with a matching condition at the inner boundary. The latter problem is readily solved in the form

$$H_1 = f(t), \quad U_1 = \frac{\Lambda \dot{f}}{\lambda_b D_0} + g_1(t) \frac{\exp(\lambda_b x)}{D_0} \tag{3.8}$$

with $g_1(t)$ an arbitrary function of time to be determined through matching.

Similarly, at the next order, one finds

$$H_2 = H_2|_{x=0} = 0, \quad U_2 = -\frac{(f + D_1) U_1}{D_0} + \frac{g_2(t) \exp(\lambda_b x)}{D_0} \tag{3.9}$$

with $g_2(t)$ a second arbitrary function of time which will also be determined through matching.

### 3.2. *The solution in the inner region:* $(x-1) \sim O(\epsilon)$, $D \sim O(\epsilon)$

Let us next define an inner independent variable $\xi$ as follows:

$$\xi = \frac{x-1}{\epsilon}, \tag{3.10}$$

and denote the dependent variables $U$, $H$, $D$ in the inner region by $u$, $h$, $d$, respectively.

The governing equations, written in terms of the inner variables, read

$$\Lambda \frac{\partial d}{\partial t} + \frac{1}{\epsilon} \frac{\partial (ud)}{\partial \xi} - \lambda_b (ud) = 0, \tag{3.11}$$

$$\Lambda \epsilon \frac{\partial u}{\partial t} + u \frac{\partial u}{\partial \xi} + \frac{1}{\epsilon} \frac{\partial h}{\partial \xi} = 0. \tag{3.12}$$

These equations must be solved with the boundary condition (2.8) at the moving boundary (the shoreline), which is readily expressed in inner variables as follows:

$$u|_{\xi = \xi_{sh}} = \Lambda \epsilon \dot{\xi}_{sh}. \tag{3.13}$$

We then expand the inner solution in the form

$$[h, u/\epsilon, d/\epsilon] = [h_1(\xi,t), u_1(\xi,t), d_1(\xi) + h_1(\xi,t)] + \epsilon[h_2(\xi,t), u_2(\xi,t), d_2(\xi) + h_2(\xi,t)] + O(\epsilon^2), \tag{3.14}$$

$$\xi_{sh} = \xi_{sh0}(t) + \epsilon\xi_{sh1}(t) + O(\epsilon^2), \tag{3.15}$$

where $\xi_{sh0}(t)$ and $\xi_{sh1}(t)$ are defined by the condition that the flow depth at the front must vanish, i.e. $d|_{\xi=\xi_{sh}} = [\epsilon(d_1+h_1) + \epsilon^2(d_2+h_2) + O(\epsilon^3)]_{\xi=\xi_{sh}} = 0$. Hence,

$$d_1|_{\xi_{sh0}} = -h_1|_{\xi_{sh0}}, \tag{3.16a}$$

$$d_2|_{\xi_{sh0}} = -h_2|_{\xi_{sh0}} - \xi_{sh1}\left.\frac{\mathrm{d}(d_1)}{\mathrm{d}\xi}\right|_{\xi_{sh0}} - \xi_{sh1}\left.\frac{\partial(h_1)}{\partial\xi}\right|_{\xi_{sh0}}. \tag{3.16b}$$

Let us now substitute from (3.14) into (3.12). At $O(1/\epsilon)$ one readily finds

$$\frac{\partial h_1}{\partial\xi} = 0 \Rightarrow h_1 = H_1 = f(t) \tag{3.17}$$

having already imposed matching. Equation (3.11) at $O(\epsilon)$ gives

$$\frac{\partial(u_1(f+d_1))}{\partial\xi} = -\Lambda\dot{h}_1 \Rightarrow u_1 = \frac{\gamma_1(t) - \Lambda\dot{f}\xi}{f+d_1}. \tag{3.18}$$

Recalling the condition (3.16*a*), we remove the singularity at the front by setting

$$\gamma_1(t) = \Lambda\xi_{sh0}\dot{f} \tag{3.19}$$

and the leading order component of the inner solution becomes

$$u_1 = \Lambda\dot{f}\frac{\xi_{sh0} - \xi}{f+d_1}. \tag{3.20}$$

The boundary condition (3.13) is readily shown to be satisfied noting that one can write

$$\dot{\xi}_{sh} = \frac{\mathrm{d}\xi_{sh}}{\mathrm{d}f}\dot{f} \tag{3.21}$$

and

$$\frac{\mathrm{d}\xi_{sh}}{\mathrm{d}f} = -\left.\left(\frac{\mathrm{d}(d_1)}{\mathrm{d}\xi} + \epsilon\frac{\mathrm{d}(d_2)}{\mathrm{d}\xi}\right)^{-1}\right|_{\xi_{sh}}. \tag{3.22}$$

At $O(\epsilon)$ one then finds

$$\frac{\mathrm{d}\xi_{sh0}}{\mathrm{d}f} = -\left.\left(\frac{\mathrm{d}(d_1)}{\mathrm{d}\xi}\right)^{-1}\right|_{\xi_{sh0}}, \quad \lim_{\xi\to\xi_{sh0}}\frac{\xi_{sh0}-\xi}{f+d_1} = -\left.\left(\frac{\mathrm{d}(d_1)}{\mathrm{d}\xi}\right)^{-1}\right|_{\xi_{sh0}}. \tag{3.23}$$

We then proceed to the next order following similar steps, to find

$$h_2 = H_2 = 0, \tag{3.24}$$

$$u_2 = -\Lambda\dot{f}\frac{\xi_{sh0}-\xi}{f+d_1}\frac{d_2}{f+d_1} + \frac{\Lambda\lambda_b\dot{f}}{f+d_1}\left[\xi_{sh0}\xi - \frac{\xi^2}{2}\right] + \frac{\gamma_2(t)}{f+d_1} \tag{3.25}$$

with $\gamma_2(t)$ arbitrary function to be determined by imposing the boundary condition at the shoreline at $O(\epsilon^2)$. The latter reads

$$u_2\left|_{\xi_{sh0}} + \xi_{sh1}\left.\frac{\partial u_1}{\partial\xi}\right|_{\xi_{sh0}} = \Lambda\dot{\xi}_{sh1}. \right. \tag{3.26}$$

Expanding (3.21) and (3.22), at $O(\epsilon^2)$ one finds

$$\dot{\xi}_{sh1} = \left[\left(\frac{\mathrm{d}(d_2)}{\mathrm{d}\xi} + \frac{\mathrm{d}^2(d_1)}{\mathrm{d}\xi^2}\xi_{sh1}\right) \Big/ \left(\frac{\mathrm{d}(d_1)^2}{\mathrm{d}\xi}\right)\right]\Bigg|_{\xi_{sh0}} \dot{f}. \tag{3.27}$$

Substituting from the latter expression into (3.26) and expanding the left-hand side in powers of $(\xi - \xi_{sh0})$ in a neighbourhood of the front, some tedious algebra shows that the landward boundary condition is indeed satisfied provided the function $\gamma_2(t)$ takes the form

$$\gamma_2(t) = \Lambda \dot{f}\left(\xi_{sh1} - \lambda_b \frac{\xi_{sh0}^2}{2}\right). \tag{3.28}$$

Equations (3.20) and (3.25) determine the velocity distribution in the inner layer up to second order, in terms of the as yet unknown quantities $\xi_{sh0}$, $\xi_{sh1}$ which (recall the condition (3.16*a*,*b*)) will be known once the shape of the equilibrium bed profile will have been determined.

### 3.3. *Matching the inner and outer solutions*

We now let $x \to 1$ in the outer solution, rewrite the resulting expression in terms of the inner variables and match it with the expression obtained letting $\xi \to -\infty$ in the inner solution.

In particular, we expand the functions $D_0(x)$ and $D_1(x)$ in a neighbourhood of the shoreline as follows:

$$D_0 = \Delta_0(1-x) + k_0(1-x)^2 + O(1-x)^3, \quad D_1 = \Delta_1(1-x) + O(1-x)^2 \tag{3.29}$$

or, in inner variables,

$$d_1 = -\Delta_0\xi, \quad d_2 = k_0\xi^2 - \Delta_1\xi. \tag{3.30}$$

At $O(\epsilon)$ matching allows us to determine the unknown function $g_1(t)$, which reads.

$$g_1(t) = -\frac{\Lambda \dot{f}}{\lambda_b \exp(\lambda_b)}. \tag{3.31}$$

Similarly, at $O(\epsilon^2)$, matching determines the function $g_2(t)$

$$g_2(t) = \Lambda \dot{f} \exp(-\lambda_b)\xi_{sh0}. \tag{3.32}$$

The outer solution then takes the following form

$$U_1 = \frac{\Lambda \dot{f}}{\lambda_b}\frac{[1 - \exp(\lambda_b(x-1))]}{D_0}, \tag{3.33}$$

$$U_2 = \Lambda \dot{f}\xi_{sh0}\frac{\exp(\lambda_b(x-1))}{D_0} - \frac{\Lambda \dot{f}}{\lambda_b}\frac{f + D_1}{D_0}\frac{[1 - \exp(\lambda_b(x-1))]}{D_0}. \tag{3.34}$$

The latter equations define the outer solution in terms of the as yet unknown shape of the equilibrium bed profile. This will be determined in the next section.

## 4. Bottom equilibrium profile and channel length

Let us now clarify the implications of equilibrium. We recall that any sediment transport law, either for bedload or for suspended load or both (e.g. Engelund & Hansen 1967), establishes a nonlinear relationship between the sediment flux and the averaged flow speed. In nature, although the forcing tide usually exhibits a dominant harmonic, further harmonic constituents concur to determine the actual form of the

tidal signal. The structure of the solution (3.33)–(3.34) then implies that, except for *ad hoc*, highly unlikely, combinations of the various harmonics composing the forcing tide, the only possible condition ensuring a null tidally averaged sediment flux is that the instantaneous flux must also vanish throughout the tidal cycle. In the real world various mechanisms cause departure from this ideal condition. Firstly, the forcing is not constant but usually varies due to astronomical, atmospheric and climatic reasons. Secondly, equilibrium is asymptotically reached and the time necessary to reach it is extremely large, being controlled by the residual component of the sediment flux which tends to vanish as equilibrium is approached: this is also readily verified from the numerical solution of the transient process whereby equilibrium is obtained (Lanzoni & Seminara 2002; Todeschini *et al.* 2008). Thirdly, in a real lagoon, channels may not be in equilibrium because flats are not in equilibrium and exchange sediments with the channels: this is the case of Venice lagoon, where dredging is periodically necessary. In other words, ideal equilibrium is never achieved in practice.

As mentioned in § 1, previous work on channel equilibrium (Friedrichs 1995) concentrated on the less stringent condition of dynamic equilibrium, whereby the maximum velocity attained in a tidal cycle is found to be spatially constant throughout the channel with values close to the critical velocity for sediment motion. This condition was also employed in a related set of models of cross-shore tidal flow allowing for a net import (export) of sediment leading to progradation (retreat) of the flat. In particular, Friedrichs & Aubrey (1996) obtained 'equilibrium' profiles for intertidal and subtidal flats by assuming that the maximum velocity in a tidal cycle was constant in space across them. This hypothesis has also found support in the numerical models of Pritchard, Hogg & Roberts (2002) and of Waeles, Le Hir & Jacinto (2004), who found that typical characteristic shear stresses at equilibrium were close to, but a little larger than, the critical shear stress for erosion.

Below, we concentrate on the problem of channel equilibrium under the condition of no sediment supply to the channel, hence we impose the static equilibrium constraint. The search for this ideal equilibrium state, besides defining a well posed problem from both the morphological and the mathematical points of view, is in fact a fundamental step to understand the response of natural systems to perturbations of the external forcing. Whether or not the system will be able to reach the asymptotic state, its trend will be to move towards a new equilibrium, the knowledge of which is then significant.

Let us then force the constraint that the maximum speed in a tidal cycle $\max|U|$ should not exceed its critical value $U_{cr}(=U^*_{cr}/\mathscr{U}^*_0)$, with $U^*_{cr}$ the critical speed for sediment motion. Note that the critical speed for the motion of cohesionless sediments depends on grain size. One may then wonder whether applying the critical constraint to the average grain size might not ensure equilibrium for the whole range of grain sizes. However, this is not a major concern as the grain size distribution of sandy bottoms typical of the outer portions of lagoon settings is fairly uniform, while the sediment becomes cohesive in the inner portions. It should also be kept in mind that, even for poorly sorted sediment mixtures, the critical stress (hence the critical speed) is only weakly dependent on grain size, due to the well-known 'hiding effect' which makes different grain sizes nearly 'equally mobile', as conclusively demonstrated by Parker, Klingeman & McLean (1982). The landward reduction of the average grain size is indeed an additional effect which is disregarded herein: it is likely to induce an additional contribution to bottom concavity, driven by the slow variation of the critical speed associated with sediment fining in the landward direction.

We then expand the equilibrium length $l^*_{eq}$ (hence the parameters $\Lambda$ and $\lambda_b$ at equilibrium) in powers of $\epsilon$ as follows:

$$(l^*_{eq},\, \Lambda,\, \lambda_b) = (l^*_{eq0},\, \Lambda_0,\, \lambda_{b0}) + (l^*_{eq1},\, \Lambda_1,\, \lambda_{b1})\epsilon + O(\epsilon^2) \tag{4.1}$$

and set

$$\epsilon\, U|_{t_M} = U_{cr}, \tag{4.2}$$

where $t_M$ is the time when $|U|$ is maximum. More specifically, $t_M = t_{M1} + \epsilon t_{M2}$, where $t_{M1}$ is the time when $|U_1|$ is maximum and $t_{M2}$ is the second-order correction. Therefore, it follows that

$$U|_{t_M} = U_1|_{\Lambda_0,\lambda_{b0},t_{M1}} + \epsilon\left[\left.\frac{\partial U_1}{\partial \Lambda}\right|_{\Lambda_0,\lambda_{b0},t_{M1}} \Lambda_1 + \left.\frac{\partial U_1}{\partial \lambda_b}\right|_{\Lambda_0,\lambda_{b0},t_{M1}} \lambda_{b1} + \left.\frac{\partial U_1}{\partial t}\right|_{\Lambda_0,\lambda_{b0},t_{M1}} t_{M2} + U_2|_{\Lambda_0,\lambda_{b0},t_{M1}}\right] + O(\epsilon^2) \tag{4.3}$$

and set

$$\epsilon\, U_1|_{\Lambda_0,\lambda_{b0},t_{M1}} = U_{cr}\,. \tag{4.4}$$

Then, since $\partial U_1/\partial t|_{t_{M1}} = 0$ by definition of maximum, the correction $D_1(x)$ is derived from the condition

$$\left.\frac{\partial U_1}{\partial \Lambda}\right|_{\Lambda_0,\lambda_{b0},t_{M1}} \Lambda_1 + \left.\frac{\partial U_1}{\partial \lambda_b}\right|_{\Lambda_0,\lambda_{b0},t_{M1}} \lambda_{b1} + U_2|_{\Lambda_0,\lambda_{b0},t_{M1}} = 0\,. \tag{4.5}$$

Recalling (3.33) it follows that the maximum value of $|U_1|$ is attained at the instant $t_{M1}$ when $|\dot{f}|$ attains its maximum. Substituting from (3.33), into (4.4), one then derives the following solution for the equilibrium bottom profile at leading order:

$$D_0(x) = \frac{l^*_b}{l^*_\infty}\left[1 - \exp\left[\frac{l^*_{eq0}}{l^*_b}(x-1)\right]\right], \quad l^*_\infty = \frac{U^*_{cr}\mathscr{D}^*_0}{a^*_0\omega^*_0|\dot{f}_{max}|} \tag{4.6}$$

with $l^*_\infty$ equilibrium length of a non-converging channel. For fixed values of the remaining parameters appearing in (4.6*b*), the value of $l^*_\infty$ increases as the relative tidal amplitude ($\epsilon = a^*_0/\mathscr{D}^*_0$) decreases.

Also note that the bed profile (4.6*a*) is a straight line in the limit $l^*_b \to \infty$ and becomes increasingly concave as $l^*_b$ decreases.

Finally, setting $D_0|_{x=0} = 1$ in (4.6*a*), we derive the leading order solution $l^*_{eq0}$ for the equilibrium length of the channel, which then allows us to determine the geometric parameters $\Delta_0$, $k_0$:

$$l^*_{eq0} = -l^*_b\, ln\left[1 - \frac{l^*_\infty}{l^*_b}\right], \quad \Delta_0 = \frac{l^*_{eq0}}{l^*_\infty}, \quad k_0 = -\left[\frac{l^*_{eq0}}{l^*_b}\right]^2 \frac{l^*_b}{2l^*_\infty}. \tag{4.7}$$

The first of these relations is plotted in figure 2(*a*) and shows that the equilibrium channel shortens as the convergence length $l^*_b$ increases and the equilibrium length of the corresponding non-converging channel, $l^*_\infty$, decreases (figure 2*b*). The latter feature describes the behaviour observed when, all the other parameters being constant, the tidal amplitude (i.e. $\epsilon$) grows or $U^*_{cr}$ decrease (see (4.6*b*)). Note that in the limit of $l^*_b$ approaching $l^*_\infty$, then figure 2(*a*) shows that $l^*_\infty/l^*_{eq0}$ tends to zero, hence $l^*_b \ll l^*_{eq0}$. However, this limit falls outside the range of validity of the present theory, constrained by the condition (3.1) whereby the parameter $\lambda_b$ must be an $O(1)$ quantity. We do not think that this fact suggests that there is a difficulty attaining static equilibrium

| Channel | $D^*_{in}$(m) | $l^*$(m) | $l^*_b$(m) | $D^*_{avg}$(m) | $r_{s\,in}$ | $l^*_{bT}$(m) | $U^*_{cr}$(m s$^{-1}$) |
|---|---|---|---|---|---|---|---|
| S. Lorenzo | 5.5 | 5375 | 4025 | 4.0 | 1 | 4722 | 0.17 |
| S. Felice | 7.0 | 15 011 | 5302 | 5.5 | 1 | 10 604 | 0.18 |
| Riga | 5.0 | 2668 | 6849 | 4.0 | 1 | 1292 | 0.17 |
| dei Bari | 6.5 | 9826 | 6858 | 5.0 | 1 | 4572 | 0.18 |
| Gaggian | 5.5 | 4381 | 3070 | 4.6 | 1 | 2558 | 0.18 |
| Scanello | 4.5 | 1698 | 924 | 3.0 | 1 | 1155 | 0.17 |
| Riga1 | 4.8 | 1744 | 3157 | 3.8 | 1 | 751 | 0.17 |
| Riga2 | 5.2 | 2379 | 3893 | 4.3 | 1 | 988 | 0.18 |

TABLE 1. Observed geometric properties of some tidal channels in Venice Lagoon. $D^*_{in}$ is the inlet depth, $l^*$ is the channel length, $l^*_b$ is the convergence length, $D^*_{avg}$ is the average channel depth, $r_{s\,in}$ is the ratio between the total (channel+shoal) and channel width at the inlet, $l^*_{bT}$ is the total convergence length, and, $U^*_{cr}$ is the threshold velocity. The characteristic values of the amplitude $a^*_0$ and of the angular frequency of the tidal wave $\omega^*_0$ within the Lagoon of Venice are 0.4 m and 1.4 $10^{-4}$ s$^{-1}$, respectively. The typical flow conductance may be calculated using the Strickler's relationship as, $k_s/\sqrt{g}\,D^{*1/6}_{avg}$, with $k_s = 35\mathrm{m}^{1/3}\mathrm{s}^{-1}$.

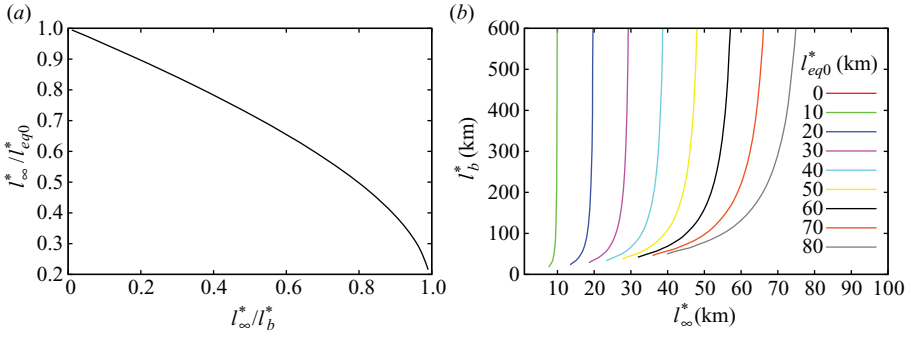


FIGURE 2. (*a*) The inverse of the equilibrium length of a channel $l^*_{eq0}$, scaled by its value $l^*_\infty$ for a non-converging channel, is plotted as a function of the inverse of the convergence length $l^*_b$, scaled by the same quantity. The plot shows that the equilibrium channel shortens as the convergence length increases. (*b*) Contour plot of the equilibrium length $l^*_{eq0}$ of channel in the $(l^*_\infty, l^*_b)$ plane.

for very strongly converging channels: in fact, equilibrium was indeed achieved by Lanzoni & Seminara (2002) on the basis of numerical simulations which were not constrained by the assumption (3.1). On the other hand, the third and fourth columns of table 1 do confirm that the latter assumption is typically verified in nature. This is not surprising: indeed, convergence arises from a very simple mechanism whereby, for bank stability, channel width must adjust to a flow depth which decreases landwards; hence, the scale of channel convergence cannot differ significantly from the scale of depth variation, which is precisely the channel length.

It is also worthwhile to observe that the outer bottom profile at equilibrium can be cast in the form

$$D_0(x) = \frac{1 - \exp[\lambda_{b0}(x-1)]}{1 - \exp(-\lambda_{b0})}. \tag{4.8}$$

We now validate our model comparing our theoretical results with experimental data (Tambroni *et al.* 2005) concerning the long-term equilibrium of a straight

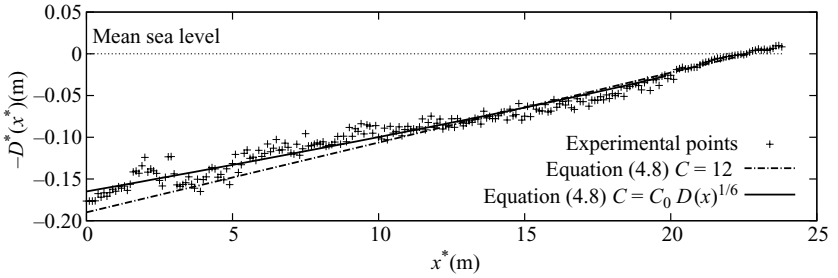


FIGURE 3. The experimental bed profile observed by Tambroni *et al.* (2005) after 2000 tidal cycles in a straight, tidal channel with constant width is compared with theoretical predictions resulting from (4.8). The relevant values of the experimental parameters are: $a_0^* = 0.024$ m, $\omega_0^* = 0.035\,\mathrm{s}^{-1}$, $l_{eq}^* = 22.9$ m, $U_{cr}^* = 0.1$ m s$^{-1}$, $C_{avg} = 12$.

erodible channel with constant width ($l_b^* \to \infty$) and no tidal flat. The morphodynamic equilibrium was approached asymptotically after about 2000 tidal cycles and was characterized by a virtually vanishing sediment flux along the entire channel. Figure 3 shows this comparison concerning the bed profile. The agreement is quite good, noting that in the constant width case, the first order contribution $D_1(x)$ vanishes identically. Note that agreement has not been achieved by fitting any of the relevant parameters, but simply adopting the values observed in the experiments and reported in Tambroni *et al.* (2005). In particular, $U_{cr}(= C\sqrt{\tau_{cr}^*/\rho}/\mathscr{W}_0^*$, with $\rho$ water density) has been estimated using the value of the critical bed shear stress for sediment motion $\tau_{cr}^*$ obtained from the Shields diagram. As regards the dimensionless Chèzy flow conductance $C$ (defined as the inverse of the square root of the friction coefficient), in figure 3 we report two profiles, the former obtained assuming a spatially constant value ($= 12$) for $C$, the latter allowing for depth dependence of $C$ according to the classical Strickler's relationship $C = C_0\, D_0^{1/6}(x)$. It appears that this dependence gives rise to a weak concavity of the bed profile which improves agreement.

The form (4.8) for the equilibrium bottom profile holds in the outer region. It matches with an inner equilibrium profile which is obtained at leading order imposing a constraint similar to (4.2) to the inner velocity (3.20). This constraint was reinforced numerically following a trial and error procedure: an inner equilibrium profile (namely an equilibrium form of $d_1(\xi)$) was guessed such to match the linear profile ($d_1(\xi) \to -\Delta_0\xi$) as $\xi \to -\infty$. A related guess was then derived for the position of the front $\xi_{sh0}(t)$. The inner velocity $u_1$ was then calculated. Next, the inner equilibrium profile $d_1(\xi)$ was corrected at each location such to satisfy the critical constraint. The new guess for $d_1(\xi)$ allowed us to update the position of the front $\xi_{sh0}(t)$ which, in turn, corrected the flow velocity requiring a new iteration. The procedure was found to converge quite rapidly to a profile which keeps linear below the intersection $\xi = 0$ between the mean water level and the bottom profile: in fact, in this region, though the time dependence of the inner velocity is no longer simply proportional to $\dot{f}$, however the maximum speed turns out to be still attained at the time when $|\dot{f}|$ attains its maximum. However, above that point, the maximum speed is associated with the speed of the front. In this region the bottom profile becomes convex. More precisely, for a sinusoidal tide, the profile predicted by Friedrichs & Aubrey (1996) was indeed confirmed as shown in the figure 4, where the presence of overtides is also accounted for and proves to have a minor effect on the shape of the equilibrium profile.

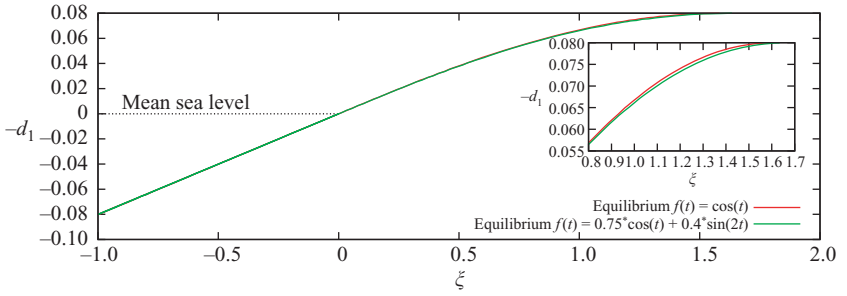


FIGURE 4. The equilibrium profile in the inner region is plotted for various forcing tides, showing that the equilibrium profile keeps linear below the point $\xi = 0$ and becomes sinusoidal above that point, thus confirming the predictions of Friedrichs & Aubrey (1996).

Having determined the function $\xi_{sh0}(t)$, the outer solution (3.34) is known and we can next impose the constraint (4.5) together with the boundary condition $D_1(0) = 0$, to obtain

$$l^*_{eq1} = l^*_{eq0}\left( f\Big|_{t_{M1}} \frac{1-\exp(-\lambda_{b0})}{\lambda_{b0}\exp(-\lambda_{b0})} - \xi_{sh0}\Big|_{t_{M1}} \right) \tag{4.9}$$

and hence the correction of the equilibrium profile

$$D_1(x) = -\, f|_{t_{M1}}\,[1 + (x-1)\exp(\lambda_{b0}x)] + \xi_{sh0}|_{t_{M1}}\,\frac{\lambda_{b0}\exp[\lambda_{b0}(x-1)]}{1-\exp(-\lambda_{b0})}x\,. \tag{4.10}$$

Note that this first-order correction is strictly null for a sinusoidal tide ($f|_{t_{M1}} = 0$, $\xi_{sh0}|_{t_{M1}} = 0$, see (3.2)), while for a generic tide allows one to derive the expression for $\Delta_1$ at equilibrium (see (3.30*b*)). Note also that $D_1$ depends on the inner solution through $\xi_{sh0}$.

## 5. The role of tidal flats at equilibrium

Tidal flats have various important roles in lagoon morphodynamics: they exchange water, sediments and nutrients with channels and salt marshes. The dynamics of tidal flats poses a complex problem as the processes of deposition and resuspension of possibly cohesive sediments due to the combined action of tidal currents and wind waves in shallow embayments are as yet not wholly understood. Here, we restrict our attention on *shoals at equilibrium* and concentrate on their major role: a storage effect on tide propagation, which will be seen to drive flow acceleration in the channel and channel shortening.

These effects can be clarified considering a simple configuration consisting of a rectangular convergent channel bounded by two identical shoals characterized by width varying in the longitudinal direction such that the total (channel+shoal) width is $B^*_T$ (figure 1*b*). With the assumption (2.1) for $B^*$, in order to account for distinct degrees of convergence of channel and shoals, we set

$$B^*_T = B^*_{T\,in}\exp\left(\frac{x^*}{l^*_{bT}}\right), \quad r_s = \frac{B^*_T}{B^*} = r_{s\,in}\exp\left[x^*\left(\frac{1}{l^*_{bT}} + \frac{1}{l^*_b}\right)\right]. \tag{5.1}$$

Denoting by $\mathscr{D}^*_s$ the scale of flow depth in the shoals, and assuming that the energy slope $J$ does not vary laterally, the ratio between the average speeds in the shoals and in the channel, computed through the Gauckler–Strickler resistance relation (i.e. $U = k_s\mathscr{D}^{*2/3}J^{1/2}$), turns out to be proportional to $[\mathscr{D}^*_s/\mathscr{D}^*_0]^{2/3}$. The ratio between

the water fluxes typically flowing in the shoals and in the channel is thus proportional to the product of the ratio $(r_s - 1)$ between their widths and the 5/3 power of the ratio between their flow depths $[\mathscr{D}_s^*/\mathscr{D}_0^*]^{5/3}$. Provided the latter product is $O(\epsilon)$, then, at least at leading order, the presence of shoals is only felt in the governing equations through the inclusion of a factor $r_s$ in the storage term of the continuity equation (3.2). The analysis then follows simply along the lines of our previous treatment, provided that the boundary condition (2.8) is replaced by

$$U|_{x=x_{sh}} = r_s \frac{\lambda}{\epsilon} \dot{x}_{sh}. \tag{5.2}$$

The expression for the flow speed at leading order then results

$$U_1 = \frac{\Lambda r_{s\,in} \dot{f}}{\lambda_{bT}} \frac{\exp(\lambda_b x)}{D_0} [\exp(\lambda_{bT}) - \exp(\lambda_{bT} x)], \tag{5.3}$$

where $\lambda_{bT}$ is defined by (2.6b) with $l_b^*$ replaced by $l_{bT}^*$. The equilibrium shape of the bed profile takes the form

$$D_0(x) = \exp(\lambda_{b0} x) \frac{1 - \exp[\lambda_{bT0}(x-1)]}{1 - \exp(-\lambda_{bT0})}, \tag{5.4}$$

where the index $_0$ stands for leading order. Finally, the channel length at equilibrium reads

$$l_{eq0}^* = l_{bT}^* ln \left[1 + \frac{l_\infty^*}{r_{s\,in} l_{bT}^*}\right]. \tag{5.5}$$

It is instructive at this stage to look at few limit cases.

The first is obtained setting $r_{s\,in} \to 1$ and, also $l_{bT}^* \to -l_b^*$ in (5.5): the previous solution (no tidal flats) is immediately recovered.

The second interesting limit is $l_{bT}^* \to \infty$ (i.e., non-convergent tidal flats adjacent to a converging channel). In this case one readily finds that the equilibrium length of the channel tends to a limit value which is a factor $r_{s\,in}$ smaller than $l_\infty^*$; on the contrary, the channel speed tends to a value a factor $r_{s\,in}$ larger than the value experienced by the same channel with no tidal flats.

The last limit is $l_{bT}^* \to -l_b^*$, hence the channel has the same degree of convergence as the adjacent tidal flats. In this case $r_s$ keeps constant and equal to $r_{s\,in}$. As a result, the channel length at equilibrium exhibits a dependence on its degree of convergence similar to that found in the absence of tidal flats, though with a major difference: $l_\infty^*$ must be replaced by $l_\infty^*/r_{s\,in}$.

We now attempt to ascertain whether the indications arising from this simple scheme do represent, at least qualitatively, the behaviour observed in the field, being aware of the unavoidable limits of this attempt, related to the complex geometries that tidal flats exhibit typically in nature. Comparison has been performed for the equilibrium bed profiles of a few channels (with adjacent flats) of Venice lagoon and is reported in figure 5. The values of the parameters employed to perform this comparison are reported in table 1, and have been determined from field measurements and analysis of topographic maps.

Note also that applying the theory developed for the no flat case to the latter data leads to unbounded values of the equilibrium lengths, suggesting that no tidal channels with the observed characteristics could exist without tidal flats. On the contrary, the simple theory presented above is able to provide reasonable predictions.

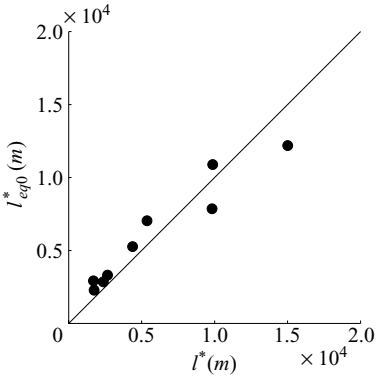


FIGURE 5. Comparisons between the observed and the equilibrium lengths, predicted by (5.5), of some tidal channels of Venice lagoon. Values of the parameters employed to perform the comparison are reported in table 1.

## 6. Discussion and concluding remarks

We have developed a theoretical approach able to predict the equilibrium length of a tidal channel in closed form. The present asymptotic scheme, having ignored the role of dissipative effects, keeps uniformly valid throughout the whole flow region. It may be of interest to analyse how wide is the region in the immediate vicinity of the front where, the local flow depth approaching zero, the role of dissipation becomes significant. Dissipative effects give rise to an additional term ($\epsilon r u|u|/c^2 d$) in the inner momentum equation (3.12), with $c$ local value of the Chèzy coefficient scaled by the reference value $C_0$ and $r$ an order one parameter. It is then clear that, $d$ and $u$ being both of $O(\epsilon)$ in the inner layer, here the dissipative term balances gravity only at $O(\epsilon^3)$. In other words dissipation plays a minor role in the inner region, everywhere except within a 'small' neighbourhood of the front. How small? Equation (3.12) again suggests that the dissipative term balances gravity at leading order within the inner layer in the region close to the front where $d$ has size $O(\epsilon^4)$. Let us make some estimate: assuming that $\epsilon \approx 0.1$, the flow depth in this region would be of the order of $10^{-4}\mathscr{D}_0^*$: with $\mathscr{D}_0^* \approx 10$ m this implies that the asymptotic scheme would fail where the flow depth does not exceed 1 mm. In this region the one-dimensional approximation is no longer meaningful. Describing this region to remove the singularity does not seem to the present authors an effort worth being pursued.

The present theoretical analysis shows that, in the absence of sediment exchange with the sea, a state of 'static' equilibrium of the channel exists such that sediment transport vanishes at each instant throughout the tidal cycle. The reader should note that the present theory only provides the equilibrium length of the channel once the inlet depth has been assigned. This approach is relevant to environments like the Lagoon of Venice, where the inlet width has been fixed artificially by the construction of jetties promoting inlet deepening to allow for steam navigation. The inlet depth is then determined by an equilibrium condition (e.g., the empirical O'Brien 1969; Jarret 1976; Marchi 1990 law). The present analysis provides some insight on a major issue, concerning the cause of the severe degradation experienced by Venice Lagoon salt marshes throughout the last century. The implication of our results can be summarized by stating that (i) on one hand inlet deepening tends to lengthen the channels; (ii) on the other hand, as the lagoon boundary imposes a constraint on channel length, the only possible response of the system to achieve equilibrium

is to widen tidal flats, i.e. erode the salt marsh area. A similar implication may be envisaged with respect to the effects of sea level rise.

In unmanaged natural systems the inlet width, as well as the channel width, is also *a priori* undefined. Hence, even with the help of O'Brien–Jarrett-Marchi law, the equilibrium length of the channel is determined by the transient process whereby, provided the initial length is larger than a threshold value, the final configuration is determined by the emersion of the sediment front propagated landwards which builds up a barrier for tide propagation (Todeschini *et al.* 2008).

Concavity of the bed profile arises from two major effects, namely channel convergence and longitudinal variations of the relative roughness. Tidal flats affect the hydrodynamics leading to flow acceleration in the channel and causing shortening of the equilibrium channel length, the more so as the flats widen.

The present work opens the way to a number of interesting developments. Let us mention two of them. The first: indications exist (Lanzoni & Seminara 2002; D'Alpaos *et al.* 2009) that an O'Brien (1969), Jarret (1976) and Marchi (1990) relationship between tidal prism $P^*$ and average cross-sectional area $\Omega^*$ of the type established for tidal inlets, namely $P^* \sim \Omega^{*6/7}$, might hold at any cross-section of a tidal channel at equilibrium. Based on the present analysis, it appears that this finding can be given some theoretical substantiation (Tambroni & Seminara 2009). The second: the morphodynamic equilibrium of estuaries differs from the one investigated above in one major respect: the upstream end is open to a steady (albeit tipically small) flux of water and sediments. How does this additional effect modify the above picture? In other words, can the analysis be extended such to cover the case of not too long estuaries?

## REFERENCES


D'Alpaos, A., Lanzoni, S., Marani, M. & Rinaldo, A. 2009 On the tidal prism – channel area relations, J. Geophys. Res., doi:10.1029/2008JF001243 (in press).

Engelund, F. & Hansen, E. 1967 A monograph on sediment transport in alluvial streams. *Danish Tech. Press*, Copenhagen .

Exner, F. M. 1925 Uber die wechselwirkung zwischen wasser und geschiebe in flussen. *Acad. Wissenscaften Wien* **134**, 165–180.

Friedrichs, C. T. 1995 Stability, shear stess and equilibrium cross-sectional geometry of sheltered tidal channels. *J. Coas. Res.* **4**, 1062–1074.

Friedrichs, C. T. & Aubrey, D. G. 1994 Tidal propagation in strongly convergent channels. *J. Geophys. Res.* **99** (C2), 3321–3336.

Friedrichs, C. T. & Aubrey, D. G. 1996 Uniform bottom shear stress and equilibrium hypsometry of intertidal flats. In *Mixing in Estuaries and Coastal Seas* (ed. C. Pattiaratchi), Coastal and Estuarine Studies, vol. 50, pp. 405–429. American Geophysical Union.

Jarret, J. T. 1976 Tidal prism-inlet area relationships. *J. Waterways Harbors Div. ASCE* **95**, 43–52.

Lanzoni, S. & Seminara, G. 2002 Long-term evolution and morphodynamic equilibrium of tidal channels. *J. Geophys. Res.* **107** (C1), 3001, doi:10.1029/2000JC000468.

Marchi, E. 1990 Sulla stabilità delle bocche lagunari a marea. *Rend. Fis. Acc. Lincei* **9**, 137–150.

Nayfeh, A. 1973 In *Perturbation Methods* (ed. H. Riffert & H. Herold). John Wiley and Sons.

Nichols, M. M. & Boon, J. D. 1994 Sediment transport processes in coastal lagoons. In *Coastal Lagoon Processes* (ed. B. Kjerfve), vol. 60, pp. 157–209. Elsevier Science.

O'Brien, M. P. 1969 Equilibrium flow areas of inlets on sandy coasts. *J. Waterways Harbors Div. ASCE* **95**, 43–52.

Parker, G., Klingeman, P. C. & McLean, D. G. 1982 Bedload and size distribution in paved gravel-bed streams. *J. Hydraul. Div.* **108** HY4, 544–571.

Pritchard, D. & Hogg, A. 2003 Cross-shore sediment transport and the equilibrium morphology of mudflats under tidal currents. *J. Geophys. Res.* **108** (C10), 3313, doi:10.1029/2002JC001570.

Pritchard, D., Hogg, A. J. & Roberts, W. 2002 Morphological modelling of intertidal mudflats: the role of cross-shore tidal currents. *Cont. Shelf Res.* **22**(11–13), 1887–1895.

Schuttelaars, H. M. & de Swart, H. E. 1996 An idealized long term morphodynamic model of a tidal embayment. *Eur. J. Mech.* B/*Fluids* **15**, 55–80.

Seminara, G. & Tubino, M. 2001 Sand bars in tidal channels. Part 1. Free bars. *J. Fluid Mech.* **440**, 49–17.

Solari, L., Seminara, G., Lanzoni, S., Marani, M. & Rinaldo, A. 2002 Sand bars in tidal channels. Part 2. Tidal meanders. *J. Fluid Mech.* **451**, 203–238.

de Swart, H. E. & Zimmermann, J. T. F. 2009 Morphodynamics of tidal inlet systems. *Annu. Rev. Fluid Mech.* **41**, 203–229.

Tambroni, N., Bolla, P. M. & Seminara, G. 2005 Laboratory observations of the morphodynamic evolution of tidal channels and tidal inlets. *J. Geophys. Res.* **110**, F04009, doi:10.1029/2004JF000243.

Tambroni, N. & Seminara, G. 2009 On the theoretical basis of O'Brien-Jarret-Marchi law for tidal inlets and tidal channels. In *Proceedings of the 6th IAHR Symposium on River, Coastal and Estuarine Morphodynamics, 21–25 September 2009* (ed. Vionnet, M. H. Garcia, E. M. Latrubesse & G. M. E. Perillo), Santa Fe, Argentina, C. A. **1**, pp. 329–335, Taylor & Francis/Balkema.

Todeschini, I., Toffolon, M. & Tubino, M. 2008 Long-term morphological evolution of funnel-shape tide-dominated estuaries. *J. Geophys. Res.* **113**, C05005, doi:10.1029/2007JC004094.

Waeles, B., Le Hir, P. & Jacinto, R. S. 2004 Modelisation morphodynamique cross-shore d un estran vaseux. *Comptes Rendus Geosci.* **336**, 1025–1033.